















































































































## Chapter 5 (Results and discussion - Composites)

### 5.1 HRSEM (High resolution Scanning Electron Microscopy)

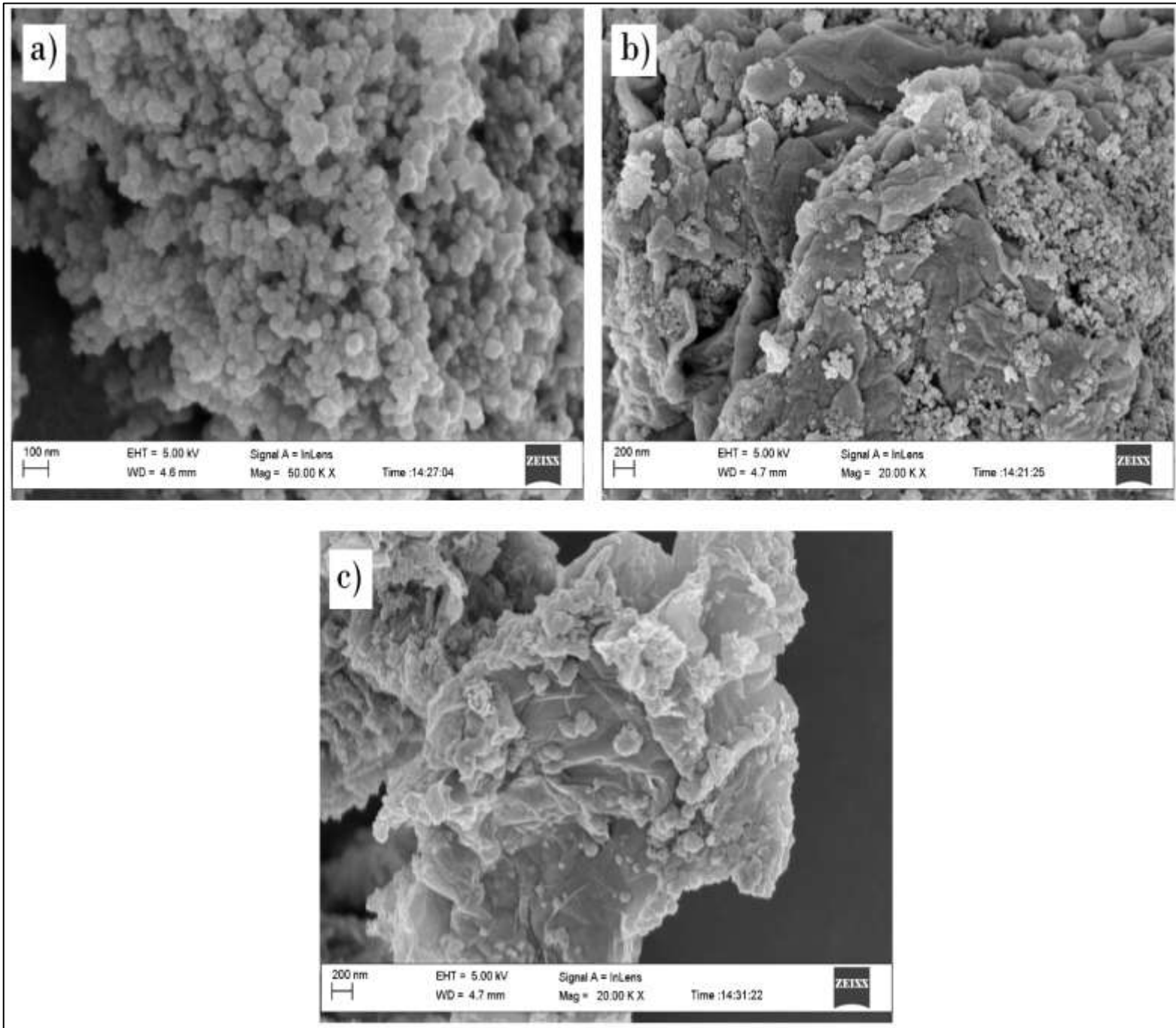


**Figure 24:** SEM images of a) AgFe- TiO<sub>2</sub>, b) rGO-AgFe-TiO<sub>2</sub> and c) AgFe-rGO nanocomposites where a) is at a magnitude of 20.00 K X and b) and c) is at a magnitude of 50.00 K X.

Figure 24 shows SEM image a) AgFe-TiO<sub>2</sub>. This can be seen similar to that of the TiO<sub>2</sub> degussa and AgFe where you find agglomerations of spherical shapes and some particles are less clustered than others. Figure 24 b) shows the SEM image of rGO-AgFe-TiO<sub>2</sub> where both the AgFe and the TiO<sub>2</sub> is seen to be intertwined with the rGO sheet-like structures. These sheet-like structures have allowed for the creation of pockets that may act as a hiding place for molecules during photocatalysis. In Figure 24 b) there are agglomerated particle structures that are lighter than others and this is an indication of the difference between the TiO<sub>2</sub> and AgFe nanoparticles. Figure 24 c) shows the SEM image of the nanocomposite AgFe-rGO. The image shows the sheet-like nature of the rGO and attached are small clusters of AgFe nanoalloy (this is seen as crumbs on the surface of the r-GO). What is evident in this image (Figure 24 c) is the brightness of those clusters. In Figure 24 a) it can be seen that there is more free space in terms of interaction during photosynthesis and this stems from the greater surface area compared to that of image b) and c) (Figure 24) where the sheet-like structures contribute to the possible hindrance in terms of its interaction with the water contaminant during photocatalysis. It is therefore speculated that photocatalysis would be carried out more efficiently with the AgFe-TiO<sub>2</sub> (image a).

The composition of each of the nanocomposites in Figure 21 AgFe-TiO<sub>2</sub>, AgFe-rGO and AgFe-TiO<sub>2</sub>-rGO was determined using EDS via SEM to confirm the elemental composition of each of the nanocomposites. This can be seen in Table 2

Element	Atomic Percentage (%)		
	AgFe-TiO <sub>2</sub>	AgFe-rGO	AgFe-TiO <sub>2</sub> -rGO
O	64.67	33.63	36.60
Ti	31.86	-	14.50
Fe	0.85	8.92	7.24
Ag	2.62	5.39	5.72
C	-	52.06	35.94
<b>Total</b>	100		

**Table 2:** Table representing the percentage elemental composition of the nanocomposites AgFe-TiO<sub>2</sub>, AgFe-rGO and AgFe-TiO<sub>2</sub>-rGO.

Table 1 represents the elemental composition percentages of the nanocomposites as confirmation for the various elements in those specific nanocomposites. For the Nanocomposite AgFe-TiO<sub>2</sub>, oxygen has the greatest percentage (64.67 %) composition due to the TiO<sub>2</sub> molecule, where there are two oxygens for every Titanium atom (31.86 %). According to the table this nanocomposite (AgFe-TiO<sub>2</sub>) contains 0.85 % Iron and 2.62 % Silver therefore indicating that the AgFe nanoalloy contains a greater percentage of silver. For the Nanocomposite AgFe-rGO the greatest percentage (52.06 %) is Carbon, which is due to the rGO and the oxygen then follows with 33.63% which also contributes to the composition of rGO. The difference between AgFe-rGO and AgFe-TiO<sub>2</sub> in terms of AgFe is the ratio of silver to Iron, according to the table, since the percentage of Iron is greater (8.92 %) than silver (5.39 %) in the nanocomposite AgFe-rGO compared to AgFe-TiO<sub>2</sub> where silver has a larger percentage than Iron. AgFe-TiO<sub>2</sub>-rGO has an elemental composition of 36.60% for oxygen which is slightly larger than carbon (35.94 %). This is due to the oxygen in TiO<sub>2</sub>, where there is a balance of two oxygen atoms per titanium (14.50 %) atom, approximately leaving an “extra” 17.61% of oxygen atoms that could be due to rGO. AgFe-TiO<sub>2</sub>-rGO does experience

the same Iron favoured ratio with an atomic percentage of 7.24 % and less so for silver having an atomic percentage of 5.72 %. These values have a significant impact on photocatalysis.

### 5.2 FTIR (Fourier Transform Infrared Spectroscopy)

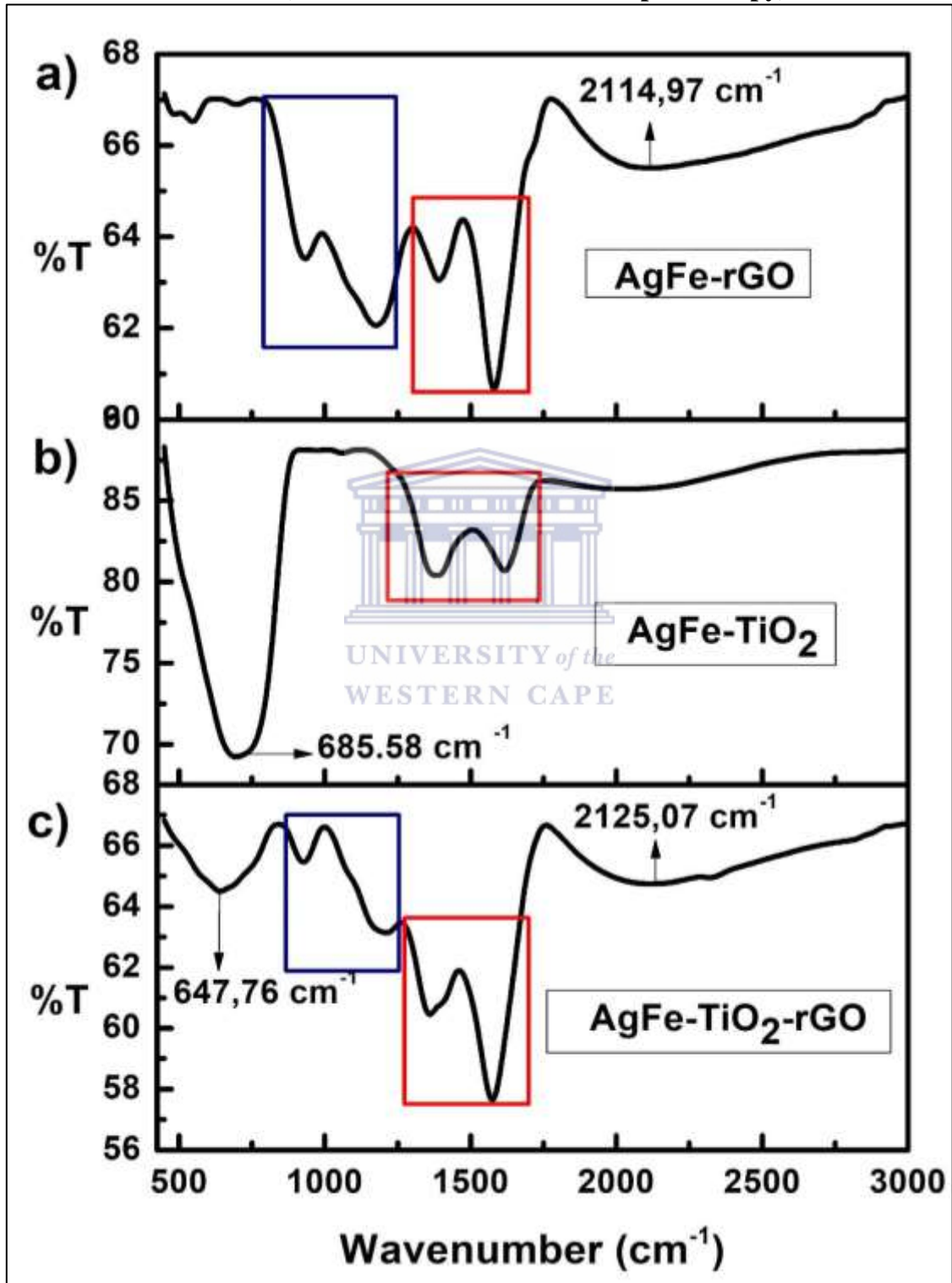


**Figure 25:** FTIR Spectra for nanocomposites a) AgFe-rGO, b) AgFe-TiO<sub>2</sub> and c) AgFe-TiO<sub>2</sub>-rGO.

Figure 25 presents the FTIR spectra for a) AgFe-rGO where a clear band is seen from about 1800  $\text{cm}^{-1}$  to 2900  $\text{cm}^{-1}$  caused by the O-H bending and stretching and this is like-wise illustrated in spectrum c) (AgFe-TiO<sub>2</sub>-rGO) therefore confirming the origin of this band to be stemmed from rGO. Spectrum a) contains a blue box inset encapsulating the band ranging from 850  $\text{cm}^{-1}$  to 1260  $\text{cm}^{-1}$  and is evident in the blue box shown in spectrum c) AgFe-TiO<sub>2</sub>-rGO. Therefore both Spectrum a) and c) is an indication of C-C bending and stretching corresponding to the rGO since graphene is made up of carbon. Figure 25 spectrum a) also contains a red box highlighting the band of range 1250  $\text{cm}^{-1}$  to about 1765  $\text{cm}^{-1}$ . This red box is observed in all three spectra which all contain AgFe, therefore concluding that this band is due to AgFe in all three nanocomposites. In spectra a), b) and c) the red box contains two bands, the one the right is roughly at 1625  $\text{cm}^{-1}$  which is due to the Fe-O bending and stretching as an indication of Fe in the nanocomposite. However in both spectra a) and c) this band is sharper than that of spectra b), this could therefore be due to the larger atomic percentage of Fe in both AgFe-rGO and AgFe-TiO<sub>2</sub>-rGO compared to AgFe-TiO<sub>2</sub>. Conversely the red box in spectrum b) contains shorter bands and the band on the left at 1370  $\text{cm}^{-1}$  (the same band in all three spectra) is sharper than that of its neighbour (at 1625  $\text{cm}^{-1}$ , owned by Fe). This in relation to Table 1 is quite possibly due to the larger atomic percentage of Ag compared to Fe in AgFe-TiO<sub>2</sub>. Spectrum b) and c) contains a band of range 500  $\text{cm}^{-1}$  to 900  $\text{cm}^{-1}$  which is due to the bending vibration of Ti-O-Ti, O-Ti-O and Ti-O bonds in the TiO<sub>2</sub> lattice. In spectrum b) this band (500 – 900  $\text{cm}^{-1}$ ) is significantly longer than that in spectrum c) which corresponds with the findings in Table 1 where there is a greater percentage of TiO<sub>2</sub> (Ti and O) in AgFe-TiO<sub>2</sub> than in AgFe-TiO<sub>2</sub>-rGO.

### 5.3 UV-vis (Ultraviolet-visible spectroscopy)

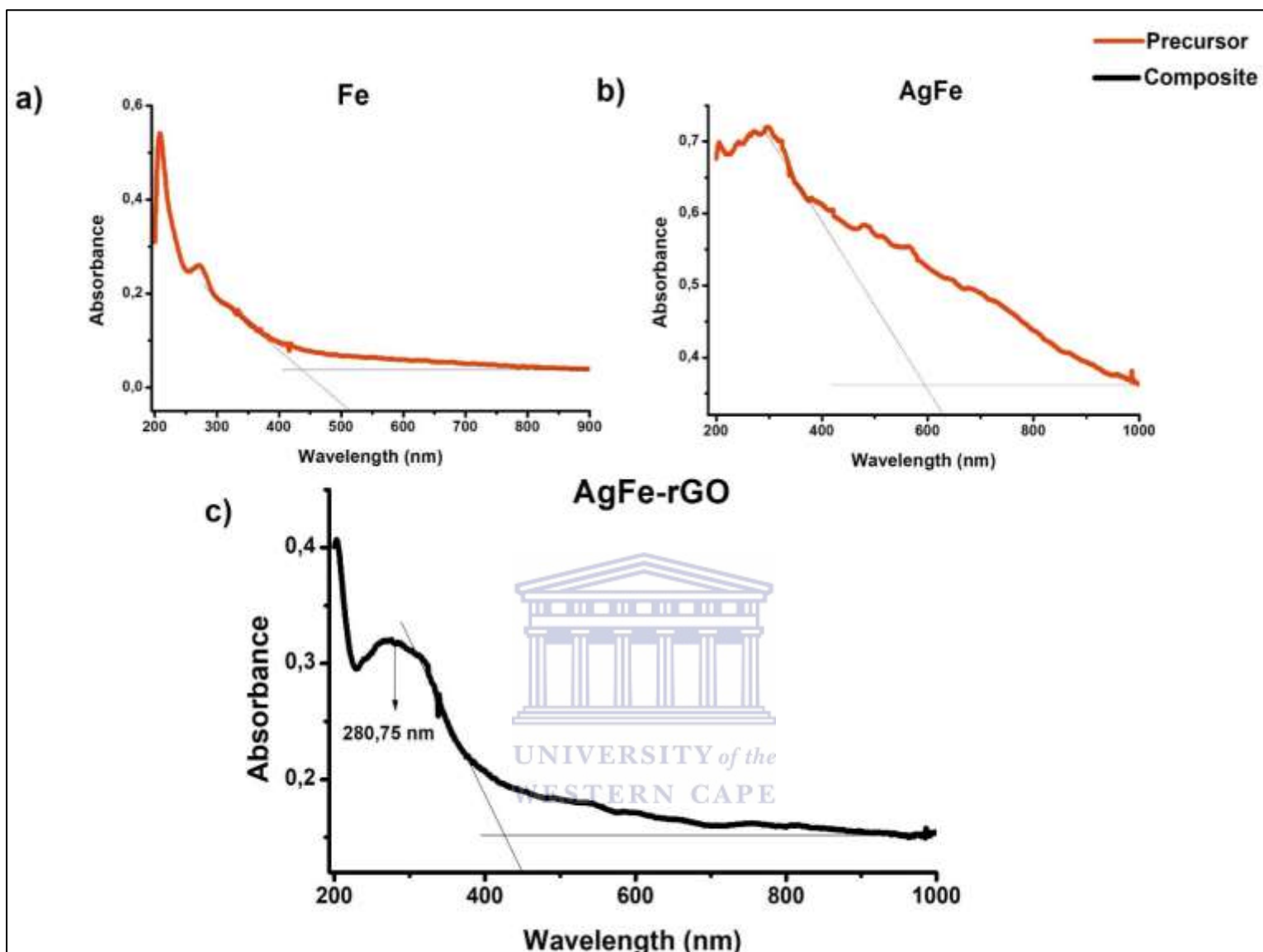


**Figure 26:** UV-vis spectra for the precursors a) Fe nanoparticles, b) AgFe nanoalloy and nanocomposite c) AgFe-rGO each with onset.

Figure 26 shows the UV-vis spectra for the nanocomposite AgFe-rGO which has a slightly broad peak at 280.75 nm similar to that of the precursor AgFe (spectrum b) which has a peak in the same range as 280.75 nm. This specific range is between 200 nm and 400 nm which is the same range as the absorbance peak for rGO as a result of the  $\pi$ - $\pi$  transitions of the aromatic C-C bonds. The band gap for the nanocomposite AgFe-rGO was calculated using the onset in

Figure 26 spectrum c) and the formula  $E = \frac{hc}{\lambda}$ . The band gap for AgFe-rGO was therefore calculated to be 2.97 eV. This is smaller than the previously calculated band gap of Fe (3.73eV) and larger than the band gap of AgFe (2.5eV). This is an indication that the AgFe-rGO may prove to decrease the photocatalytic ability of TiO<sub>2</sub> in the nanocomposite AgFe-TiO<sub>2</sub>-rGO.

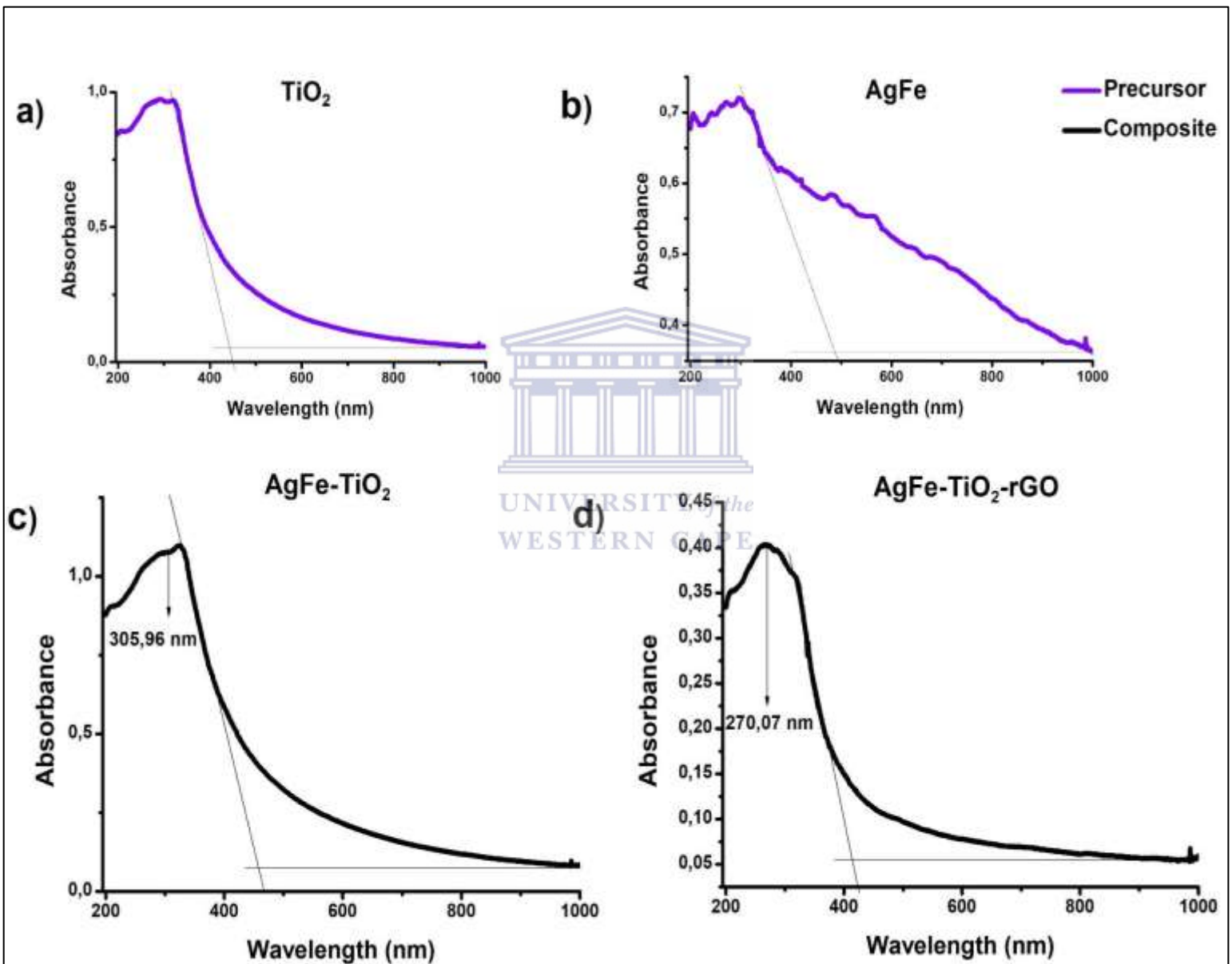


**Figure 27:** UV-vis spectra for the precursors a) TiO<sub>2</sub> (Degussa), b) AgFe nanoalloy, nanocomposites c) AgFe-TiO<sub>2</sub> and d) AgFe-TiO<sub>2</sub>-rGO each with onset.

Figure 27 shows the UV-vis spectra for the nanocomposites c) AgFe-TiO<sub>2</sub> and d) AgFe-TiO<sub>2</sub>-rGO. In Figure 27 c) there is a peak that is in the same range (200 nm – 400 nm) as that of the peak for the a) TiO<sub>2</sub> precursor, however the difference is the ultimately the very slight shift in the peak (shift to the right/ which is essentially a red shift) of c) AgFe-TiO<sub>2</sub>, this correlates with the band gap which was calculated to be 2.77 eV. For figure 27 d) the same is evident compared to c) where the peak occurs in the same range (200 nm – 400 nm) as a) TiO<sub>2</sub> precursor, however it displays a slight shift (to the left/a blue shift) of the peak, this correlates with the band gap which was calculated to be 3.02 eV. This therefore means that the b) AgFe (with a band gap of 2.5 eV) has caused the improvement of the photocatalytic reactivity of a) TiO<sub>2</sub>, however that the rGO seems to have worked against the b) AgFe nanoalloy since it increased the band gap tremendously.



## 5.4 XRD (X-ray Diffraction)

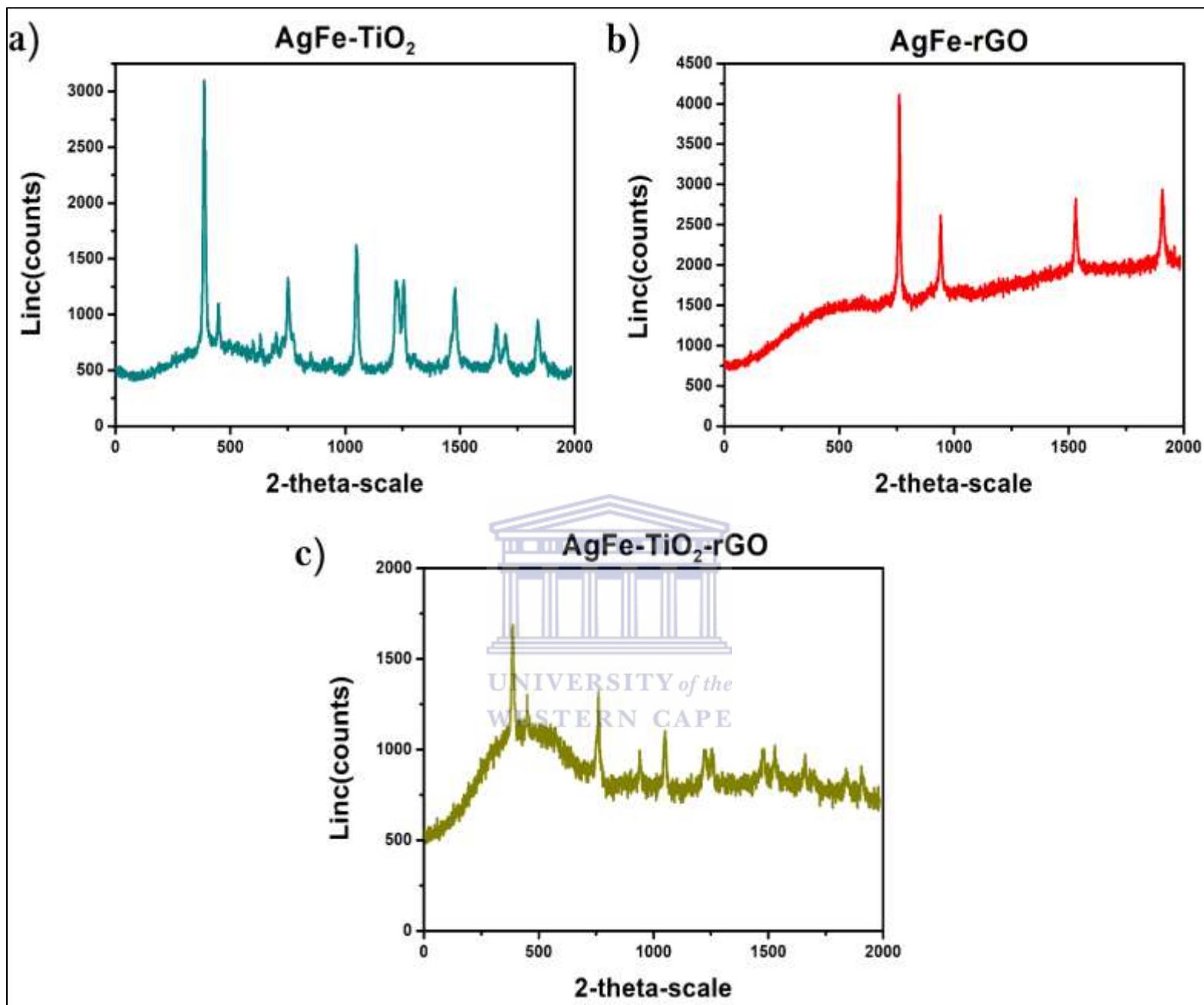
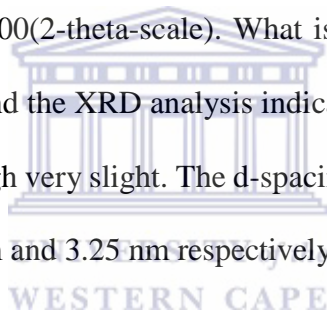


**Figure 28:** X-ray diffraction (XRD) patterns of the nanomposite samples a) AgFe-TiO<sub>2</sub>, b) AgFe-rGO and c) AgFe-TiO<sub>2</sub>-rGO.

Figure 28 shows the XRD patterns of a) AgFe-TiO<sub>2</sub> and according to the analysis the composite contains both Ag and Fe similar to that of patterns found in figure 21 a) and d) which show the XRD patterns of TiO<sub>2</sub> degussa and AgFe respectively. Therefore this also confirms the crystallinity of the composite. The XRD patterns in Figure 28 c) AgFe-TiO<sub>2</sub>-rGO are similar to that found in Figure 28 a) AgFe-TiO<sub>2</sub> which therefore confirms the presence of Ag, Fe and TiO<sub>2</sub>. However the peaks are observed to be sharper in Figure 28 a) AgFe-TiO<sub>2</sub> compared to that of the peaks in c) AgFe-TiO<sub>2</sub>-rGO and since the crystallinity of a) AgFe-TiO<sub>2</sub> is confirmed through the peaks the crystallinity is somewhat challenged in the composite c) AgFe-TiO<sub>2</sub>-rGO where you can see a broad peak in the results around 500(2-theta-scale), and this is due to the reduced graphene oxide (rGO). This same effect is seen in the composite b) AgFe-rGO where the same broad peak is seen at 500(2-theta-scale). What is also seen in b) AgFe-rGO is the slight shift in peaks to the right and the XRD analysis indicate that there are peaks confirming the presence of Ag and Fe although very slight. The d-spacing for AgFe-TiO<sub>2</sub> and AgFe-TiO<sub>2</sub>-rGO was calculated to be 2.22 nm and 3.25 nm respectively.



### 5.5 CV (Cyclic voltammetry)

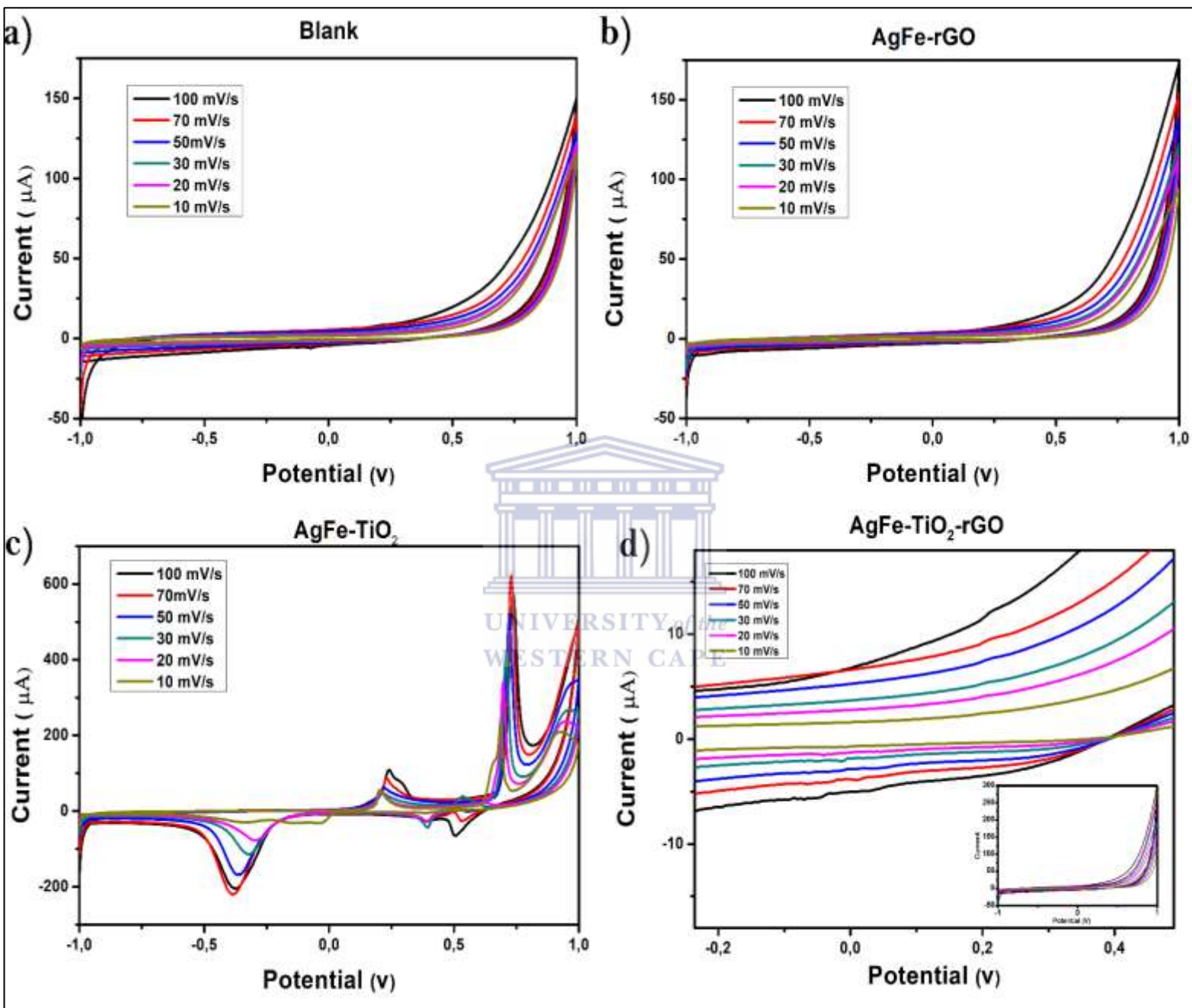


**Figure 29:** CV graph of a) Blank of glassy carbon electrode, nanocomposites b) 100 mg AgFe-rGO, c) 100 mg AgFe- TiO<sub>2</sub> and d) 100 mg AgFe-TiO<sub>2</sub>-rGO with insert in 5M LiOH electrolyte at scan rates 10 mV/s, 20 mV/s, 30 mV/s, 50 mV/ s, 70 mV/s and 10 mV/s in 5M LiOH electrolyte on a glassy carbon electrode.

Scan Rate (mV.s <sup>-1</sup> )	Scan Rate <sup>1/2</sup> (mV.s <sup>-1</sup> )	I <sub>pc</sub> (μA)	I <sub>pa</sub> (μA)	E <sub>pa</sub> (V)	E <sub>pc</sub> (V)	ΔE <sub>p</sub> (V)
10	3.16	0.46	3.52	0.217	-0.054	0.271
20	4.47	0.61	3.52	0.213	-0.054	0.267
30	5.48	0.74	3.58	0.213	-0.052	0.265
50	6.32	1.06	6.58	0.215	-0.054	0.269
70	8.37	1.54	5.36	0.217	-0.052	0.269
100	10	1.98	8.73	0.215	-0.054	0.269
<b>Mean</b>		<b>1.07</b>	<b>5.22</b>	<b>0.215</b>	<b>-0.053</b>	<b>0.268</b>

**Table 3:** Scan rate vs Scan Rate<sup>1/2</sup> (mV.s<sup>-1</sup>) vs I<sub>pc</sub>, I<sub>pa</sub>, E<sub>pa</sub> and E<sub>pc</sub> for AgFe-TiO<sub>2</sub>-rGO

Determination of reversibility:

$$\frac{I_{pa}}{I_{pc}} = \frac{5.22 \mu A}{1.07 \mu A}$$

$$= 4.88 \mu A$$

$$\therefore -\frac{I_{pa}}{I_{pc}} \approx 1 \dots \textit{therefore it is chemically irreversible}$$

Determination of Diffusion Coefficient:

$$D^{1/2} = \frac{j_p}{2.72 \times 10^5 \times n^{3/2} \times A \times C_0 \nu^{1/2}}$$

$$D^{1/2}_{(AgFe-TiO_2-rGO)} = \frac{\frac{150.85 A}{m^2}}{2.72 \times 10^5 \times \frac{3}{2} \times 0.071 m^2 \times 5 M \times 0.1^{\frac{1}{2}}}$$

$$D^{1/2}_{(AgFe-TiO_2-rGO)} = 4.94 \times 10^{-3}$$

$$D_{(AgFe-TiO_2-rGO)} = 2.44 \times 10^{-5} \text{ cm}^2 \cdot \text{s}^{-1}$$

Scan Rate (mV.s <sup>-1</sup> )	Scan Rate <sup>1/2</sup> (mV.s <sup>-1</sup> )	I <sub>pc</sub> (μA)	I <sub>pa</sub> (μA)	E <sub>pa</sub> (V)	E <sub>pc</sub> (V)	ΔE <sub>p</sub> (V)
10	3.16	14.66	94.06	0.20	0.39	-0.19
20	4.47	199.18	92.17	0.20	0.39	-0.19
30	5.48	127.64	94.58	0.21	0.39	-0.18
50	6.32	131.7	96.72	0.21	0.39	-0.18
70	8.37	148.24	103.1	0.23	0.40	-0.17
100	10	153.09	145.53	0.24	0.39	-0.15
<b>Mean</b>		<b>129.10</b>	<b>104.3</b>	<b>0.22</b>	<b>0.39</b>	<b>-0.18</b>

**Table 4:** Scan rate vs Scan Rate<sup>1/2</sup> (mV.s<sup>-1</sup>) vs vs I<sub>pc</sub>, I<sub>pa</sub>, E<sub>pa</sub> and E<sub>pc</sub> for AgFe-TiO<sub>2</sub>

**Determination of reversibility:**

$$\frac{I_{pa}}{I_{pc}} = \frac{104 \mu A}{129.10 \mu A}$$

$$= 0.81 \mu A$$

$$\therefore -\frac{I_{pa}}{I_{pc}} \approx 1 \dots \text{therefore it is chemically reversible}$$



**Determination of Diffusion Coefficient:**

$$D^{1/2} = \frac{j_p}{2.72 \times 10^5 \times n^{3/2} \times A \times C_0 \nu^{1/2}}$$

$$D^{1/2}_{(AgFe-TiO_2)} = \frac{\frac{149.31 A}{m^2}}{2.72 \times 10^5 \times \frac{3}{2} \times 0.071 m^2 \times 5 M \times 0.1^{\frac{1}{2}}}$$

$$D^{1/2}_{(AgFe-TiO_2)} = 4.89 \times 10^{-3} \times 2.25 \times 10^{-3}$$

$$D_{(AgFe-TiO_2)} = 2.39 \times 10^{-5} \text{ cm}^2 \cdot \text{s}^{-1}$$

Figure 29 shows CV graph for a) Blank of glassy carbon electrode, nanocomposites b) AgFe-rGO, c) AgFe- TiO<sub>2</sub> and d) AgFe-TiO<sub>2</sub>-rGO with insert. Figure 29 b) AgFe-rGO doesn't display any peaks, however compared to a) blank there is an increase in current with increase in scan rates where 100 mV/s has the highest current in b). Figure 29 c) displays two oxidation (anodic) peaks and two reduction (cathodic) peaks and this is due to the oxidation states of Fe. What is also observed (Figure 29 c) is the increase in peak current with increase in scan rate with 100 mV/s having the highest peaks for both oxidation and reduction. Figure 29 d) AgFe-TiO<sub>2</sub>-rGO has an insert that is zoomed out CV graph of AgFe-TiO<sub>2</sub>-rGO and when compared to a) shows no peaks but does display an increase in current with increase in scan rate, with the 100 mV/s having the highest current. Since the zoomed out graph (Figure 29 c) insert) contains no peak it was zoomed into to display the peaks that is seen in Figure 29 c) where the peak increases with increase in scan rate. From graph c (AgFe-TiO<sub>2</sub>) to graph d (AgFe-TiO<sub>2</sub>-rGO) the peaks can be seen to have drastically decreased indicating the effect rGO has on the composite which is the decrease oxidation and reduction peaks resulting in the decrease in transfer of electrons. The estimated  $\Delta E_p$  for a) Bare GCE, c) AgFe-TiO<sub>2</sub> and d) AgFe-TiO<sub>2</sub>-rGO is 0.25 V, 1.06 V and 0.268 V respectively. This facilitates the enhanced conduction pathways with the modified catalysts, with AgFe-TiO<sub>2</sub> having the highest electron kinetic transport. The diffusion coefficient for AgFe-TiO<sub>2</sub>-rGO and AgFe was  $2.44 \times 10^{-5} \text{ cm}^2 \cdot \text{s}^{-1}$  and  $2.39 \times 10^{-5} \text{ cm}^2 \cdot \text{s}^{-1}$  respectively. This is roughly the same and is an indication of the similarity of the diffusion that might occur in each of these composites.

## Chapter 6 (Photocatalytic study)

### Optimization of photocatalysis system

The concentration of pollutant and solution pH may impact on their removal from contaminated water. Therefore it was necessary to investigate the effect of these two parameters on the degradation of orange II dye that was selected as the model pollutant.

#### 6.1 Effect of initial concentration of Dye (Orange II)

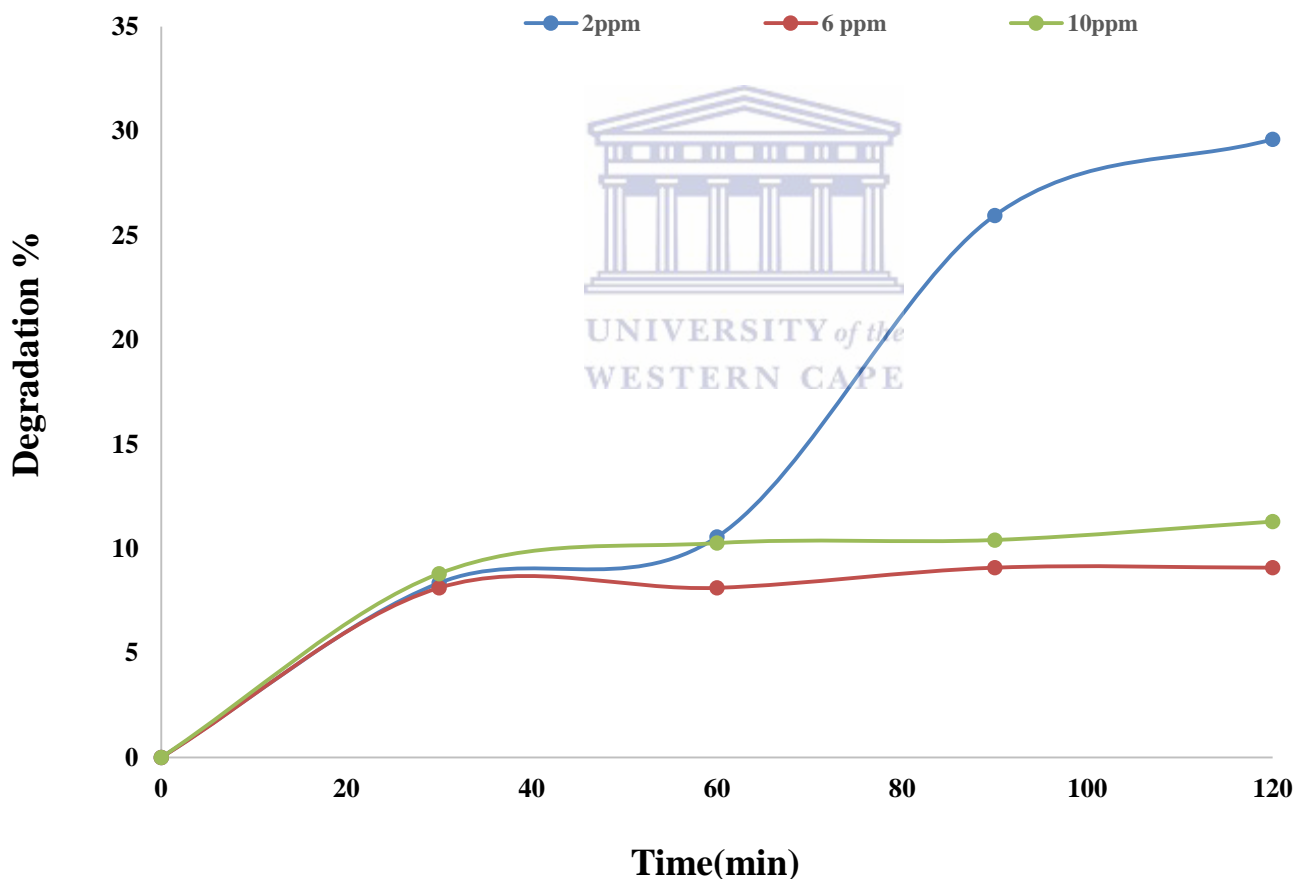


**Figure 30:** Graph illustrating the effect of concentration on the dye (Orange II) degradation percentage at the following conditions. Varied parameters: Dye concentration from 2, 6 to 10 ppm. Fixed parameters: pH, solution volume 500 ml, irradiation time 120 min, distance between lamp and solution 5cm.

Figure 30 presents the effect of initial concentration of dye on the degradation percentage at the applied conditions. Though literature sustains that the initial concentration of the pollutant has an impact on its removal from polluted water. That is, the degradation percentage of the pollutant may decrease with increase of its initial concentration (Reza, Kurny, & Gulshan, 2017). So from the results plotted in figure 30 the trend between initial concentration and percentage degradation claimed in the literature was not observed. Nevertheless, higher removal of orange (II) was achieved at lower concentration 2 ppm. For example at minute 90 concentration 10, 6 and 2ppm had 10, 8 and 27% degradation respectively. Even though 2 ppm appeared as the best concentration in this case a reasonable concentration of dye needed to be defined to meet the sensitivity conditions of the extended analytical method such as HPLC analysis, therefore 4ppm was chosen as the working concentration of orange (II) used throughout all experiments conducted in this photocatalysis study.

Apart from dye concentration the effect of solution pH on orange (II) degradation percentage was also investigated.

## 6.2 Effect of solution pH on Dye (Orange II)

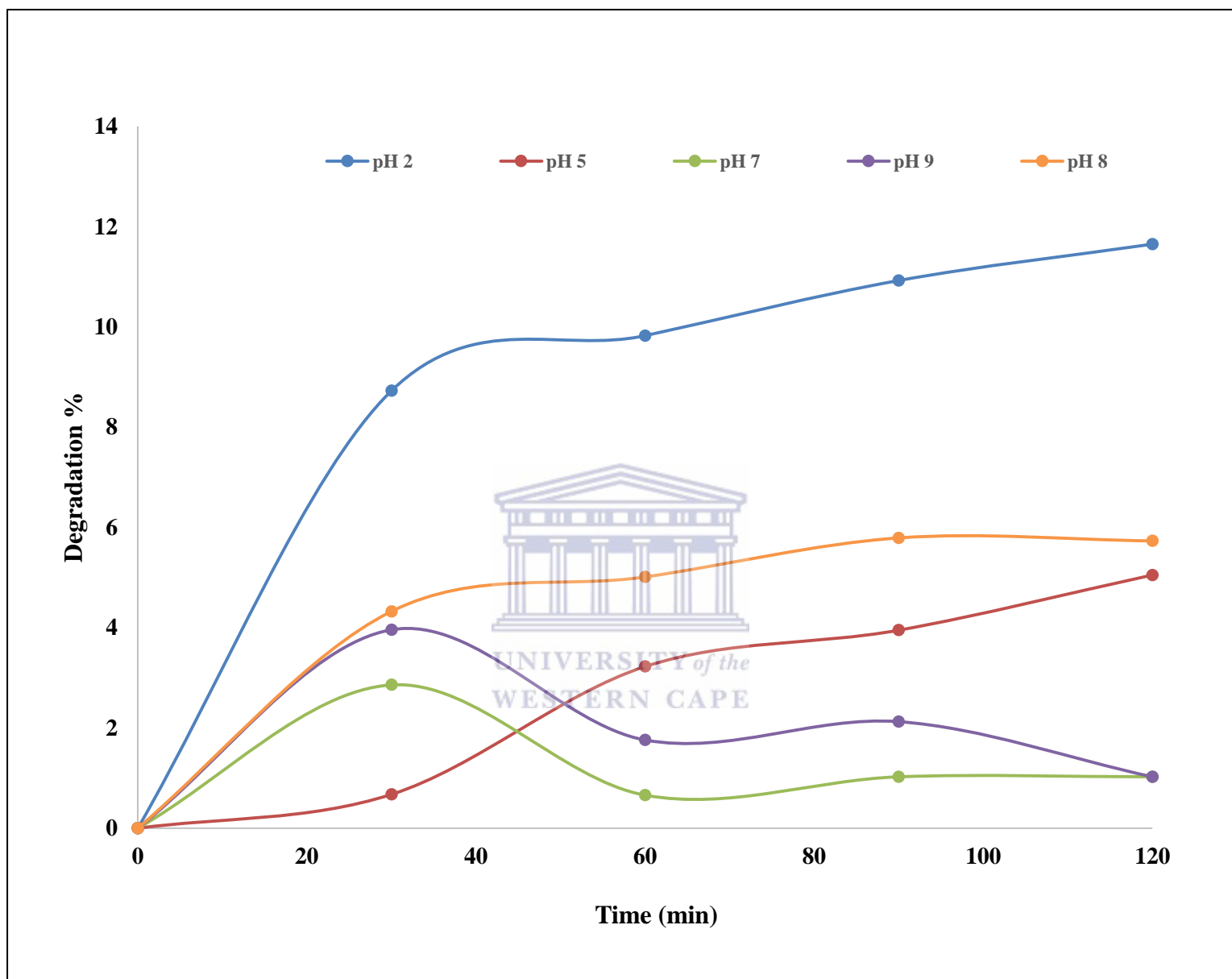
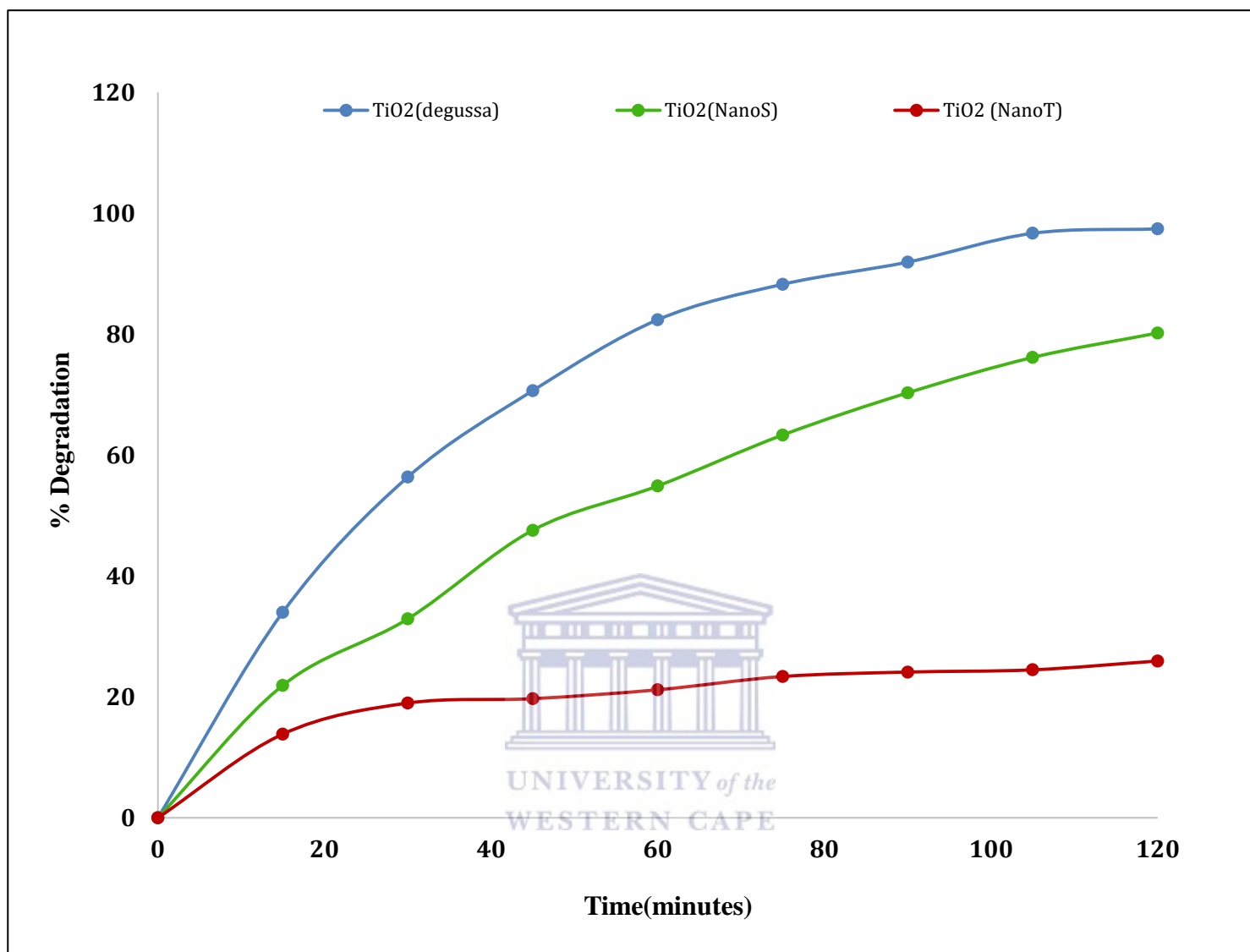


**Figure 31:** Graph illustrating the effect of solution pH on orange II degradation percentage at the following condition. Varied parameters: Solution pH from 2, 5 to 9. Fixed parameters: Dye concentration 4ppm, solution volume 500ml, irradiation time 120 min and distance between lamp 5cm.

Figure 31 presents the effect of solution pH on dye percentage removal at the applied conditions. According to literature pH may effect percentage degradation (Reza et al., 2017). That is, the degradation percentage of pollutant may increase with a decrease in solution pH. In Figure 31 there is however no consistent observable trend, nevertheless at the highest pH values the lowest percentage degradation was observed and at the lowest, pH 2, experienced the greatest percentage degradation. Second to pH 2 was pH 8 and this is because the base used (NaOH) to establish the pH had an influence on the percentage degradation (likewise with pH 9) as well as the temperature. It was also observed that pH 5 presents a percentage degradation below that of pH 8 and that correlates with the trend stated in literature. An example of this can be seen at minute 60 where pH 2, 5, 7, 8 and 9 had degradation percentages of 9.83, 3.23, 0.66, 5.01 and 1.76 respectively. Thus pH 2 appeared as the best pH for percentage degradation for the pollutant Orange (II). Therefore pH 2 was used as a working pH of Orange (II) and throughout all experiment conducted in this photocatalyst study.

After the photocatalysis system was optimized the following parameters dye concentration 4ppm, solution pH 2 were chosen as optimum factors that were associated to fixed parameters. Including solution volume 500 ml, irradiation time 2 hours, distance between lamp and solution 5 cm. Therefore the aforementioned optimum conditions were used to assess the photocatalytic activity of the catalysts (TiO<sub>2</sub> Degussa, TiO<sub>2</sub> Nano spheres, TiO<sub>2</sub> nanotubes) and the effect of catalyst dosage on the degradation percentage of dye, respectively.

### 6.3 Photocatalytic degradation effect of the catalysts on Dye (Orange II)



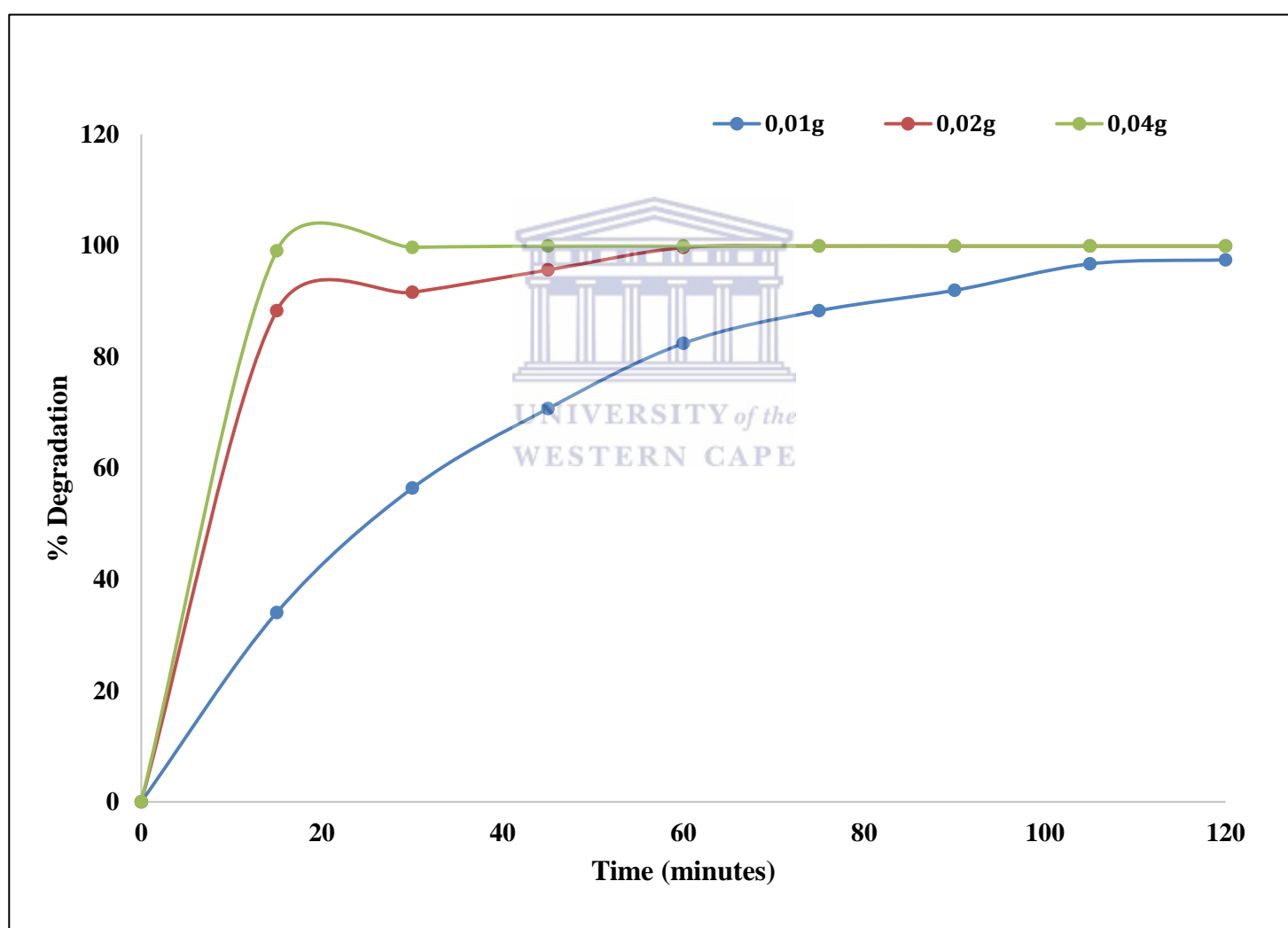
**Figure 32:** Graph illustrating the photocatalytic activity of TiO<sub>2</sub> (TiO<sub>2</sub> Degussa, TiO<sub>2</sub> nanospheres, TiO<sub>2</sub> nanotubes based catalysts) on dye degradation percentage at the following experimental conditions. Solution pH 2, concentration 4ppm, mass of catalyst 0.01g, solution volume 500ml, irradiation time 2hours, distance between lamp and solution 5cm.

Figure 32 presents the photocatalytic activity of the catalysts (TiO<sub>2</sub> Degussa, TiO<sub>2</sub> nanospheres, and TiO<sub>2</sub> nanotubes) under the established optimum conditions. It is observed that TiO<sub>2</sub> degussa had the highest percentage degradation and TiO<sub>2</sub> had the lowest percentage degradation. An example of this can be seen at minute 60 TiO<sub>2</sub> Degussa, TiO<sub>2</sub> nanospheres and

TiO<sub>2</sub> nanotubes had degradation of 82.41%, 54.91% and 21.19% respectively. This is due to the size of the nanoparticles and in turn its dispersion in the Orange (II) solution. Therefore TiO<sub>2</sub> was selected as the best catalyst for this photocatalytic study.

Since TiO<sub>2</sub> degussa was the best catalyst for the degradation of Orange (II) in this study, the impact of its amount on degradation percentage of dye was also investigated.

#### 6.4 Effect of photocatalyst dosage on dye (orange II) degradation efficiency



**Figure 33:** Illustration of the effect of TiO<sub>2</sub> (Degussa) dosage on percentage degradation of dye. Experimental conditions. Varied parameters: Mass of TiO<sub>2</sub> (Degussa) 0.01g, 0.02g and 0.04g. Fixed parameters: solution pH 2, concentration 4ppm, solution volume 500ml, irradiation time 2hours, distance between lamp and solution 5cm.

Figure 33 presents the effect of photocatalyst dosage on Orange (II) percentage degradation. Literature sustains that the mass of the catalyst has an impact on its removal (Reza et al., 2017). That is the degradation percentage of the pollutant increases with increase in mass/dosage of  $\text{TiO}_2$  (Reza et al., 2017). So from the results plotted in Figure 33 the trend between mass of catalyst and percentage degradation was observed to confirm that. An example of this trend is observed at minute 30 where 0.01g, 0.02g and 0.04g of  $\text{TiO}_2$  observed degradations of 56.38%, 91.57% and 99.67% respectively. Therefore it was observed that the higher the dosage of  $\text{TiO}_2$  the greater the percentage degradation.

### 6.5 Effect of different photocatalyst on Orange II dye degradation

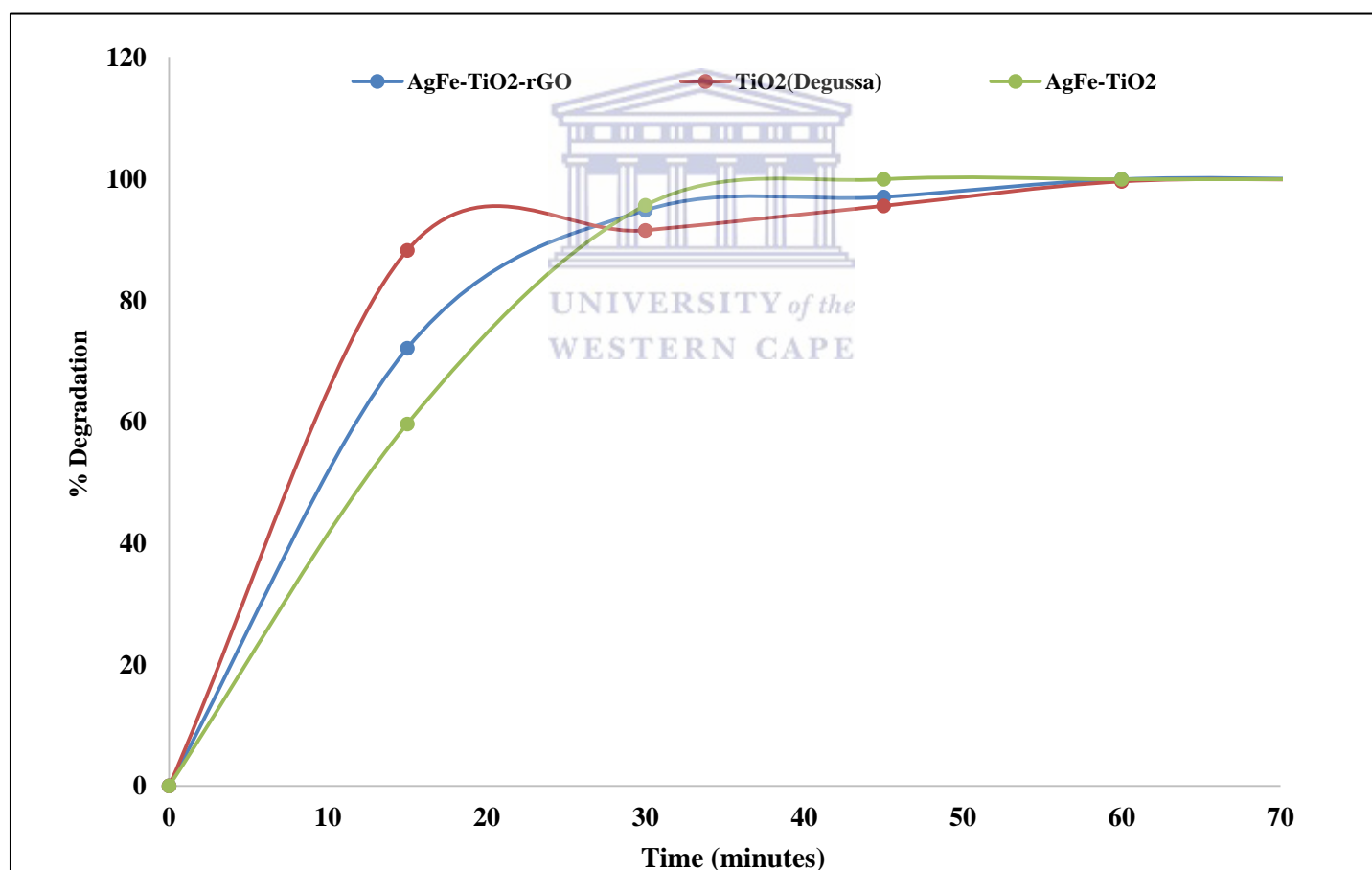


**Figure 34:** Illustration of the effect of the different photocatalysts  $\text{TiO}_2$  (Degussa),  $\text{AgFe-TiO}_2$  and  $\text{AgFe-TiO}_2\text{-rGO}$  on percentage degradation of dye. Experimental conditions. Fixed parameters: solution pH 2, concentration 4ppm, solution volume 500ml, irradiation time 2hours, distance between lamp and solution 5cm and 0.04g of each photocatalyst.

Figure 34 presents the effect of the different photocatalysts on Orange (II) percentage degradation. The degradation percentage of the pollutant should increase with all three photocatalysts. So from the results plotted in Figure 34 the trend between the type of photocatalyst and percentage degradation, the following was observed. From 0 – 30 minutes the TiO<sub>2</sub> degussa degraded the dye at a faster rate than both AgFe-TiO<sub>2</sub> and AgFe-TiO<sub>2</sub>-rGO with AgFe-TiO<sub>2</sub> reacting the slowest with the dye. This is due to the surface area of the TiO<sub>2</sub> degussa that is greater than that of the AgFe-TiO<sub>2</sub> and AgFe-TiO<sub>2</sub>-rGO. However the faster degradation of the dye via the photocatalyst AgFe-TiO<sub>2</sub>-rGO compared to the AgFe-TiO<sub>2</sub> photocatalyst is due to the pockets that were formed in the nanocomposite of AgFe-TiO<sub>2</sub>-rGO (observed in Figure 24 b) which would allow for the Orange II dye molecules/particles to be stored inside instead of being photocatalysed which allows for the misguided observation that it seems to be the better photocatalyst of the two when in actual fact that result does not correlate with that of the findings of UV which through calculation indicated that the band gap of AgFe-TiO<sub>2</sub> and AgFe-TiO<sub>2</sub>-rGO were 2.77 eV and 3.02 eV respectively implying that the better photocatalyst is AgFe-TiO<sub>2</sub>. That however is confirmed from 30 -70 minutes where it is observed that the best photocatalyst is AgFe-TiO<sub>2</sub>, and the weakest is the TiO<sub>2</sub> degussa, which has a UV band gap of 2.93 eV, and compared to AgFe-TiO<sub>2</sub>-rGO (UV band gap of 3.02 eV) should be weaker, but as mentioned this could be caused by the rGO pockets created in the AgFe-TiO<sub>2</sub>-rGO nanocomposite. Therefore it was observed that the AgFe-TiO<sub>2</sub> photocatalyst displayed the best overall photocatalytic activity.

## Chapter 7

### 7.1 Conclusion

The aim of this project was to investigate Titanium dioxide modified by creating a two composites using the nanobimetal/nanoalloy silver-iron (AgFe) and reduced graphene oxide (rGO) as an improved photocatalyst for removal of contaminants such as dye from water. Different Titanium Dioxide (TiO<sub>2</sub>) was synthesised using a hydrothermal method and TiO<sub>2</sub> degussa (the purchased TiO<sub>2</sub> nanopowder) was used as the best form of the catalyst, since it illustrated faster photocatalysis during the photocatalytic study. The TiO<sub>2</sub> degussa contained nanoparticles of size 15 nm – 25 nm. These dimensions would prove to enhance the dispersion of the photocatalyst in the water and therefore increase its possible collision, and in turn increase its reactivity. However its interaction affinity and reactivity efficiency can be further enhanced through the addition of the nanomaterials silver-iron alloy and possibly reduced graphene oxide. The nanocomposites AgFe-TiO<sub>2</sub> and AgFe-TiO<sub>2</sub>-rGO were successfully synthesised and was evident in the morphological studies. The anatase phase of the TiO<sub>2</sub> degussa and nanocomposites AgFe-TiO<sub>2</sub> and AgFe-TiO<sub>2</sub>-rGO were confirmed through XRD and FTIR therefore serving as a support for the maintained phase of the TiO<sub>2</sub> even after modification. The d-spacing for AgFe-TiO<sub>2</sub> and AgFe-TiO<sub>2</sub>-rGO was calculated to be 2.22 nm and 3.25 nm, which favoured AgFe-TiO<sub>2</sub> in terms of photocatalysis. The XRD results along with HRTEM further indicate that both are crystalline in nature where AgFe-TiO<sub>2</sub> shows a higher degree of crystallinity due to the rGO in AgFe-TiO<sub>2</sub>-rGO which is amorphous. The diffusion coefficients for TiO<sub>2</sub>, AgFe-TiO<sub>2</sub>-rGO and AgFe-TiO<sub>2</sub> were  $9.07 \times 10^{-7} \text{ cm}^2 \cdot \text{s}^{-1}$ ,  $2.44 \times 10^{-5} \text{ cm}^2 \cdot \text{s}^{-1}$  and  $2.39 \times 10^{-5} \text{ cm}^2 \cdot \text{s}^{-1}$  respectively. FTIR confirmed the presence of the AgFe nanoalloy in both AgFe-TiO<sub>2</sub> and AgFe-TiO<sub>2</sub>-rGO as well as the rGO in AgFe-TiO<sub>2</sub>-rGO. FTIR along with HRSEM-EDS confirmed that the precursor TiO<sub>2</sub> degussa and nanocomposites AgFe-TiO<sub>2</sub> and AgFe-TiO<sub>2</sub>-rGO contained both Silver, Iron, Titanium and oxygen along with carbon (for graphene), where there was a silver favoured silver:Iron percentage ratio (0.85 % : 2.62 %) in AgFe-TiO<sub>2</sub> than in AgFe-TiO<sub>2</sub>-rGO (5.72% : 7.24%) which was also confirmed in FTIR where at the band range of 1250 cm<sup>-1</sup> - 1765 cm<sup>-1</sup> (red box) contained shorter bands and the first band in the double banded filled red box (1250 cm<sup>-1</sup> - 1765 cm<sup>-1</sup> band range) was longer (since there was a higher silver percentage in the

silver : iron ratio) than the left which was the opposite in the spectrum of AgFe-TiO<sub>2</sub>-rGO where the second band in the double banded filled red box (1250 cm<sup>-1</sup> - 1765 cm<sup>-1</sup> band range) was longer/shaper than the other and this indicated an iron favoured silver : iron percentage ratio. This has proved to be significant during the photocatalytic study. HRSEM has also confirmed the morphology of AgFe-TiO<sub>2</sub> and AgFe-TiO<sub>2</sub>-rGO where it was evident that AgFe-TiO<sub>2</sub> had a more agglomerated spherical morphology compared to AgFe-TiO<sub>2</sub>-rGO where there were sheet-like rGO structures that created pockets that could cause potential “mistaken- photocatalysis” (where the photocatalyst appeared to be reacting more effectively with the catalyst when in actual fact the dye particles weren’t being converted into free radicals but in this case hidden/stored in the rGO formed pockets giving the idea/misinterpretation of photocatalysis). This was confirmed in the photocatalytic study where the AgFe-TiO<sub>2</sub>-rGO behaved “better” than AgFe-TiO<sub>2</sub> initially (first 30 minutes in Figure 33) but was however the opposite for the rest of the time (1h 30 minutes). This was further confirmed with UV where the band gap for AgFe-TiO<sub>2</sub>-rGO was 3.02 eV compared to AgFe-TiO<sub>2</sub> which had a band gap of 2.77 eV therefore indicating that AgFe-TiO<sub>2</sub> would be the better photocatalyst. This was confirmed in the photocatalytic study where AgFe-TiO<sub>2</sub> was proven as the best catalyst to convert the dye (Orange II) into free radicals and ultimately remove the contaminant from the water compared to AgFe-TiO<sub>2</sub>-rGO.

## 7.2 Future work

GC/MS spectroscopy is needed to identify the intermediates and final products of the dye (Orange II) degradation as well as a hydroxyl radical formation study to ensure the efficiency of the photocatalyst. HRTEM which was used cannot determine the bimetallic nature of the AgFe bimetal. In future work Brunauer –Emmett-Teller (BET) analysis will be carried out to determine the specific surface area of the materials. Those results may be used to further prove the above mechanism for enhanced photocatalysis. The Dye (Orange II) was used as an organic contaminant in this study however further study into inorganic contaminants such as nitrates, which present health concerns in rural areas with groundwater being the main source of water, may be employed to further test the efficiency of the proposed photocatalyst.

## REFERENCES

- 1) Von Bormann, T. and Gulati, M. The Food Energy Water Nexus:WWF-SA, (2014)
- 2) Zyoud, Ahed, et al. "Optimizing photo-mineralization of aqueous methyl orange by nano-ZnO catalyst under simulated natural conditions." *Journal of Environmental Health Science and Engineering* 13.1 (2015): 46.
- 3) Methyl orange, Material safety data sheet, statement of hazardous nature. sc-206030: (2011)
- 4) Eljiedi, Arwa Alseddig Ahmed, and Azlan Kamari. "Removal of methyl orange and methylene blue dyes from aqueous solution using lala clam (*Orbicularia orbiculata*) shell." *AIP Conference Proceedings*. Vol. 1847. No. 1. AIP Publishing, (2017).
- 5) Awuah E., Nyarko K.B., Owusu P.A., & Osei-Bonsu K. *Desalination*, 248, (2009): 453-459.
- 6) Chong MN, Jin B, Chow CW, Saint C. *Water Res.* 44, (2010): 2997–3027.
- 7) Gaya UI, Abdullah AH. *J Photochem Photobiol A Chem.* 9: (2008) 1–12
- 8) Zhu K., Neale N. R., Miedaner A. and Frank A. J., *Nano Lett.* 7: (2007), 69–74
- 9) Beranek R., Tsuchiya H., Sugishima T., Macak J. M., Taveira L., Fujimoto S., Kisch H. and Schmuki P., *Appl.Phys. Lett.* 87: (2005), 243114
- 10) Roy P., Berger S. and Schmuki P., *Angew. Chem. Int. Ed.* 50: (2005), 2904–2939
- 11) Lazar MA, Varghese S, Nair SS. *Catalysts.* 2: (2004), 572–601.
- 12) Takeuchi M., Yamashita H., Matsuoka M., Anpo M., Hirao T., Itoh N., and Iwamoto N., *Catal. Lett.* 67: (2000) 135.

- 13) Linsebigler A. L., Lu G., and Yates J. T. Jr., *Chemical Reviews*, 95, 3: (1995), 735–758
- 14) Pável C. Hernández D. C, Saúl R. M., Facundo R., *Soft Nanoscience Letters*. 4: (2014), 53-62.
- 15) Li W, Shah, S. I. Huang, C. P, Jung, O, Ni, C. *Mater. Sci. Eng. B* 96, 247. (2002).
- 16) Fernández-García, M, Martínez-Arias, A, Hanson, J. C, Rodríguez, J. A. *Chem. Rev.* 104: (2014), 4063.
- 17) Ai B, Duan X, Sun H, Qiu X, Wang S. *Catal. Today*, in press, (2015).
- 18) Liu J, Huang J.H, Zhou H, Antonietti M. *ACS Appl. Mater. Interfaces*. 6: (2015), 8434–8440
- 19) Wang X., Maeda K., Chen X., Takanabe K., Domen K., Hou Y., Fu X., Antonietti M., *Journal of the American Chemical Society*. 131: (2010), 1680.
- 20) Yan H., Yang H., *Journal of Alloys and Compounds*. 509, L26, (2011).
- 21) Adekoya O. D, Muhammad T, Nor A. S. A., *Malaysian Journal of Fundamental and Applied Sciences*. 11,3, (2015) : 102-105.
- 22) Zheng, Z. K, Huang, B. B, Qin, X. Y, Zhang, X. Y, Dai, Y, Whangbo, M. H., *J. Mater. Chem.* 21: (2011): 9079–9087.
- 23) Liang, W. J, Li, J, Jin, Y. Q. *Build. Environ.* 51: (2012), 345–350.
- 24) Sondra Ayadi, Cristian Perca, and Ludovic Legrand, *Nanoscale Res Lett.* 8(1): (2013), 95

- 25) Yanfeng Chen, Weixin Huang, Donglin He, Yue Situ, and Hong Huang, ACS Appl. Mater. Interface: **(2014)**, 14405–14414
- 26) Umehayashi T, Yamaki T, Itoh H. and Asai K., J. Phys. Chem. Solids. 63 : **(2002)**, 1909–1920.
- 27) Y. K. Lai, H. F. Zhuang, K. P. Xie, D. G. Gong, Y. X. Tang, L. Sun, C. J. Lin and Z. Chen, New J. Chem.34: **(2010)**, 1335–1340.
- 28) Zhu J, Zheng W, He B, Zhang J. and Anpo M., J. Hazard. Mater. 216: **(2004)**, 35–43
- 29) Zhou, M, Yu, J, Cheng, B., J. Hazard. Mater. 137: **(2006)**, 1838–1847.
- 30) Mishra T. , Mahato M. ,Noor Aman, J. Patel, N, Sahu. R. K. Catal. Sci. Technol. 1: **(2011)**, 609-615.
- 31) Markowska-Szczupak A, Ulfing K, & Morawski A. W. Catalysis Today. 169, 1: **(2011)**, 249-257.
- 32) Ohno T, Sarukawa K, Tokieda K, and Matsumura M. Journal of Catalysis. 203: **(2001)**, 82-86.
- 33) Cong Y, Zhang J, Chen F. Journal of Physical Chemistry C. 111: **(2007)**, 10618–10623
- 34) Serpone N, Journal of Physical Chemistry B. 110: **(2006)**, 24287– 24293.
- 35) Ping Lei, Feng Wang, Xiaowei Gao, Yanfen Ding, Shimin Zhang, Jincui Zhao, Shaoren Liu, Mingshu Yang., Journal of Hazardous Materials: **(2013)**, 227–228, 185–194,
- 36) Khan, Mohammad Mansoob, Syed Farooq Adil, and Abdullah Al-Mayouf. "Metal oxides as photocatalysts." **(2015)**: 462-464.
- 37) Ping. C, Zhi. Y , Hong. W, Wei. C , Mingxia. C, Wenfeng .S, Guifu D. international journal of hydrogen energy .37: **(2012)**, 2224 -2230

- 38) Akwensiogbe, Mbinze. The influence of anthropogenic nitrate on groundwater quality in the Thaba Nchu area. Diss. University of the Free State, (2012).
- 39) Reiner, Monika. "Industrial waste minimisation in South Africa: A case study in the textile and metal finishing sectors by." (2002).
- 40) Helmer, Richard, Ivanildo Hespanhol, and World Health Organization. "Water pollution control: a guide to the use of water quality management principles." (1997).
- 41) Woodford, Chris, Calhoun, Yael, Seideman, David, Environmental chemistry module 1. "Water Pollution." (2015)
- 42) Enderlein, Rainer, Williams. "Water quality control". (1997)
- 43) Su, Claire Xin-Hui, et al. "Combination and hybridisation of treatments in dye wastewater treatment: a review." *Journal of Environmental Chemical Engineering* 4.3 (2016): 3618-3631.
- 44) Yadav, V. S. K., and M. K. Purkait. "Concurrent electrochemical CO<sub>2</sub> reduction to HCOOH and methylene blue removal on metal electrodes." *RSC Advances* 6.47 (2016): 40916-40922.
- 45) Li, Fu, et al. "Enhanced removal of azo dye using modified PAN nanofibrous membrane Fe complexes with adsorption/visible-driven photocatalysis bifunctional roles." *Applied Surface Science* 404 (2017): 206-215.
- 46) Gadekar, Mahesh R., and M. Mansoor Ahammed. "Coagulation/flocculation process for dye removal using water treatment residuals: modelling through artificial neural networks." *Desalination and Water Treatment* 57.55 (2016): 26392-26400.
- 47) Félicien, Mazille. "Coagulation-Flocculation". (2003)

- 48) Granche, Berhe. "Removal of colour and turbidity (coagulation, flocculation filtration)". (2015)
- 49) Ajmal, Anila, et al. "Principles and mechanisms of photocatalytic dye degradation on TiO<sub>2</sub> based photocatalysts: a comparative overview." *Rsc Advances* 4.70 (2014): 37003-37026.
- 50) Shi, Jianwen, et al. "Photocatalytic degradation of methyl orange in water by samarium-doped TiO<sub>2</sub>." *Environmental Engineering Science* 25.4 (2008): 489-496.
- 51) Wold, Aaron. "Photocatalytic properties of titanium dioxide (TiO<sub>2</sub>)." *Chemistry of Materials* 5.3 (1993): 280-283.
- 52) Elsalamony, R. A. "Research & Reviews: Journal of Material Sciences." (2016)
- 53) Kobwittaya, K., and S. Sirivithayapakorn. "Photocatalytic Reduction of Nitrate over Fe-modified TiO<sub>2</sub>." *APCBEE Procedia* 10 (2014): 321-325.
- 54) Kobwittaya, Krisana, and Sanya Sirivithayapakorn. "Photocatalytic reduction of nitrate over TiO<sub>2</sub> and Ag-modified TiO<sub>2</sub>." *Journal of Saudi chemical society* 18.4 (2014): 291-298.
- 55) Bharti, Bandna, et al. "Formation of oxygen vacancies and Ti<sup>3+</sup> state in TiO<sub>2</sub> thin film and enhanced optical properties by air plasma treatment." *Scientific reports* 6 (2016)
- 56) Ansari, Sajid Ali, et al. "Silver nanoparticles and defect-induced visible light photocatalytic and photoelectrochemical performance of Ag@ m-TiO<sub>2</sub> nanocomposite." *Solar Energy Materials and Solar Cells* 141 (2015): 162-170.
- 57) Kumari, R. Mankamna, et al. "Antibacterial and photocatalytic degradation efficacy of silver nanoparticles biosynthesized using *Cordia dichotoma* leaf extract." *Advances in Natural Sciences: Nanoscience and Nanotechnology* 7.4 (2016): 045009.

- 58) Jang, Jum Suk, et al. "Development of a potential Fe<sub>2</sub>O<sub>3</sub>-based photocatalyst thin film for water oxidation by scanning electrochemical microscopy: effects of Ag– Fe<sub>2</sub>O<sub>3</sub> nanocomposite and Sn doping." *Chemistry of Materials* 21.20 (2009): 4803-4810.
- 59) Pan, Xuan, et al. "TiO<sub>2</sub>/graphene nanocomposite for photocatalytic application." *Materials and Processes for Energy: Communicating Current Research and Technological Developments; Méndez-Vilas, A., Ed* (2013): 913-920.
- 60) Alam, Tanvir E. "Metal Oxide Graphene Nanocomposites for Organic and Heavy Metal Remediation." (2012).
- 61) Nanakoudis. M, What is SEM? SEM technology explained, PhenomWorld, 01 Jun (2017)
- 62) Maleki. S, TEM, Idolunion, 01 Apr (2010)
- 63) Khalil, Munawar, et al. "Electrodeposition of Iridium Oxide Nanoparticles for pH Sensing Electrodes." *Journal of The Electrochemical Society* 163.9 (2016): B485-B490.
- 64) Winterburn. E, "Braggs", Wordpress, 06 Feb (2013)
- 65) Riding. T, "Graphene", Lorentin, 4 Jan (2011)
- 66) Schwarz, James A., Cristian I. Contescu, and Karol Putyera, eds. *Dekker encyclopedia of nanoscience and nanotechnology*. Vol. 3. CRC press, (2004)
- 67) Bakan, Feray, et al. "Structural and Chemical Analysis of Hydroxyapatite (HA)-Boron Nitride (BN) Nanocomposites Sintered Under Different Atmospheric Conditions." *Microscopy and Microanalysis* 23.5 (2017): 891-899.

- 68) Fresno, F., et al. "Influence of surface density on the CO<sub>2</sub> photoreduction activity of a DC magnetron sputtered TiO<sub>2</sub> catalyst." *Applied Catalysis B: Environmental* 224 (2018): 912-918.
- 69) Pal, Jolly, et al. "Removal of methyl orange by activated carbon modified by silver nanoparticles." *Applied Water Science* 3.2 (2013): 367-374.
- 70) Kumar, A., and G. Pandey. "A Review on the Factors Affecting the Photocatalytic Degradation of Hazardous Materials." *Material Sci & Eng Int J* 1.3 (2017): 00018.
- 71) Theivasanthi, Thirugnanasambandan, and Marimuthu Alagar. "Titanium dioxide (TiO<sub>2</sub>) Nanoparticles XRD Analyses: An Insight." arXiv preprint arXiv (2013):1307.1091

